Synthesis of PPEGMEA-*g*-PMAA densely grafted double hydrophilic copolymer and its use as a template for the preparation of size-controlled superparamagnetic Fe_3O_4/polymer nano-composites†

Lina Gu,[a] Zhong Shen,[a] Chun Feng,[a] Yaogong Li,[a] Guolin Lu,[a] Xiaoyu Huang,*[a] Guowei Wang[b] and Junlian Huang*[b]

Received 7th April 2008, Accepted 3rd July 2008
First published as an Advance Article on the web 4th August 2008
DOI: 10.1039/b805841e

A series of well-defined amphiphilic densely grafted copolymers, containing polyacrylate backbone, hydrophobic poly(methoxymethyl methacrylate) and hydrophilic poly(ethylene glycol) side chains, were synthesized by successive atom transfer radical polymerization. Poly[poly(ethylene glycol) methyl ether acrylate] comb copolymer was firstly prepared *via* the grafting-through strategy. Next, poly[poly(ethylene glycol) methyl ether acrylate]-*g*-poly(methoxymethyl methacrylate) amphiphilic graft copolymers were synthesized *via* the grafting-from route. Poly(methoxymethyl methacrylate) side chains were connected to the polyacrylate backbone through stable C–C bonds instead of ester connections. The molecular weights of both the backbone and the side chains were controllable and the molecular weight distributions were in the range 1.38–1.42. Poly(methoxymethyl methacrylate) side chains were selectively hydrolyzed under mild conditions without affecting the polyacrylate backbone to obtain the final product, poly[poly(ethylene glycol) methyl ether acrylate]-*g*-poly(methacrylic acid) densely grafted double hydrophilic copolymer. Finally, these double hydrophilic copolymers were used as templates to prepare superparamagnetic Fe_3O_4/polymer nano-composites with narrow size distributions *via* an *in situ* co-precipitation process, which were characterized by FT-IR, TGA, DLS and X-ray diffraction in detail. The size of the nano-composites can be controlled in a certain range by adjusting the length of the poly(methacrylic acid) side chains and the weight ratio of copolymer to Fe_3O_4 nano-particle used.

Introduction

Double hydrophilic copolymers (DHCs) are a new class of amphiphilic copolymer, which consist of two different hydrophilic segments. Recently, double hydrophilic copolymers have attracted more attention since they can form aqueous micellar systems making them more environmentally friendly and biocompatible compared to micelles formed in organic media.[1–4] When the micelles were formed by double hydrophilic copolymers in water, one hydrophilic segment becomes hydrophobic accompanied by physical or chemical transformations, while another hydrophilic segment remains soluble in aqueous media.[5–14] The typical hydrophilic segments used in double hydrophilic copolymers include poly(ethylene glycol),[5–8] poly(acrylic acid) (PAA),[5,9] poly(methacrylic acid),[6,10] poly(styrene sulfonic acid),[11] poly(*N*-isopropylacrylamide),[12] poly(*N*-alkylaminoethyl methacrylate),[8,9,12] polyoxazoline,[13] poly(vinyl pyridine),[6] poly(vinyl ethers),[14] polypeptides and RNA.[7]

In the past few years, the self-association studies of double hydrophilic copolymers have mainly focused on linear block copolymers.[1,5–11,13,14] But, the architecture of the copolymers is also important for the properties of the micelles. It has been found that the properties of the micelles formed by nonlinear block copolymers are fundamentally different from those of linear copolymers.[12] Graft copolymers can bring additional complexity in the studies of solution association since that they have confined and complicated structures.[15,16] So, the studies of the self-assembly behavior of graft copolymers can provide more information about the control of micellar morphology and the design of new nano-materials.

Due to the development of living radical polymerization, including atom transfer radical polymerization (ATRP)[17–20] and modified ATRP,[21–24] new structural graft polymer can be designed and conveniently synthesized now. Densely grafted copolymer is a kind of copolymer with an intriguing structure.[25,26] More complex densely grafted copolymers with two hydrophobic double-grafted brushes have been reported.[27–29] Our group also synthesized a kind of amphiphilic double-grafted copolymer containing two different kinds of side chains.[30] But, the double hydrophilic densely grafted copolymer with two different water-soluble double-grafted brushes has been never reported. Generally, poly(ethylene glycol) (PEG) is chosen as one hydrophilic segment due to its excellent solubility and wide applications.[31,32] Poly(methacrylic acid) (PMAA) is selected as

[a]*Laboratory of Polymer Materials and Key Laboratory of Organofluorine Chemistry, Shanghai Institute of Organic Chemistry, Chinese Academy of Sciences, 354 Fenglin Road, Shanghai 200032, P. R. China. E-mail: xyhuang@mail.sioc.ac.cn; Fax: +86-21-64166128; Tel: +86-21-54925310*
[b]*The Key Laboratory of Molecular Engineering of Polymer, State Education Ministry of China, Department of Macromolecular Science, Fudan University, 220 Handan Road, Shanghai 200433, P. R. China*
† Electronic supplementary information (ESI) available: Experimental section. See DOI: 10.1039/b805841e

another hydrophilic segment since PMAA is a kind of weak polyelectrolyte and its ionization degree is governed by the pH and ionic strength of the aqueous solution.[6,10]

Moreover, double hydrophilic block copolymers bearing two different hydrophilic segments can be used as surfactants to prepare core–shell iron oxide nano-particles.[33–36] The preparation of composite magnetic nano-particles has gained increasing attention due to its emerging applications such as sensors, imaging agents, storage media and catalysis in the fields of biotechnology and microelectronics. These inorganic–organic hybrids are particularly interesting since they inherit properties of both polymer and inorganic material. In addition, the coated polymer can effectively prevent the aggregation of particles. Among the typical magnetic nano-particles, Fe_3O_4 magnetite, whose biocompatibility has been proven, is a promising candidate to prepare inorganic–organic hybrids. Copolymers containing carboxylic acid groups have been investigated as an approach to prepare and stabilize iron oxide nano-particles.[37] Polymer-coated magnetite nano-particles were prepared by co-precipitation of Fe^{2+} and Fe^{3+} in the presence of copolymers containing PEG and PAA/PMAA segments since the PEG segment can impart biocompatibility and increase the half-life of nano-particles.[38,39]

In this article, we synthesized a series of well-defined densely grafted double hydrophilic copolymers *via* the "grafting-from" strategy (Scheme 1). Poly[poly(ethylene glycol) methyl ether acrylate]-*g*-poly(methoxymethyl methacrylate) amphiphilic densely grafted copolymer was synthesized *via* successive ATRP. Poly[poly(ethylene glycol) methyl ether acrylate]-*g*-poly (methacrylic acid) double hydrophilic copolymer was obtained from the selective hydrolysis of poly(methoxymethyl methacrylate) (PMOMMA) side chains.

These copolymers were used as a template to prepare superparamagnetic Fe_3O_4/polymer nano-composites with narrow size distribution *via* an *in situ* co-precipitation process. The compact structure of the graft copolymer consisting of 15 PEG-*b*-PMAA chains and 5 PEG chains linked by stable covalent bonds is expected to stabilize the nano-particles and prevent unfavorable aggregation since the side chains can protect the formed single particle.

Results and discussion

Synthesis and characterization of PPEGMEA-Br 2 macroinitiator

Poly[poly(ethylene glycol) methyl ether acrylate] (PPEGMEA **1**) comb copolymer was prepared *via* ATRP of PPEGMEA macromonomer using Me_6TREN as a ligand, detailed characterization can be found in our previous report.[30] Successful

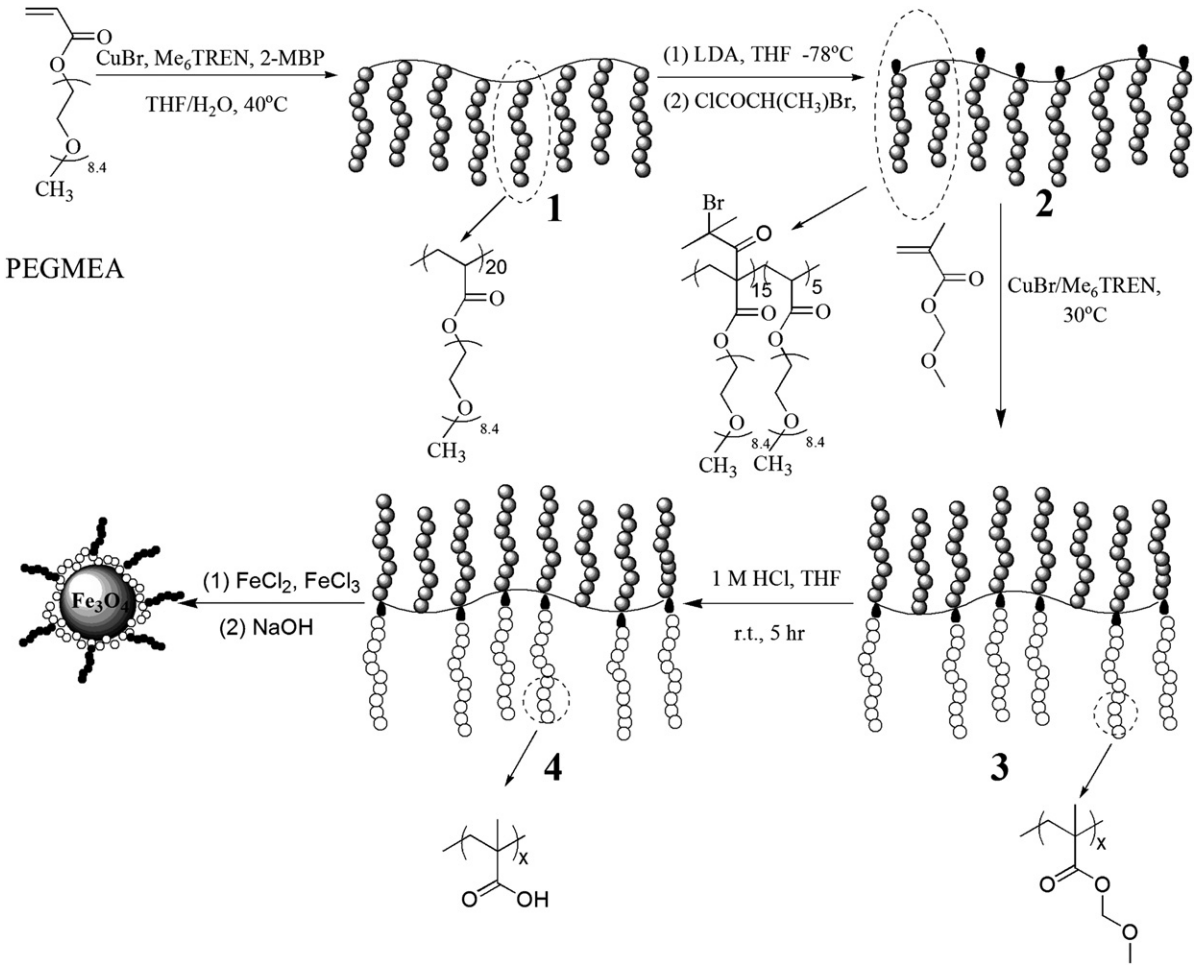

Scheme 1 Preparation of superparamagnetic Fe_3O_4/polymer nano-composites with PPEGMEA-*g*-PMAA densely grafted double hydrophilic copolymer as a template.

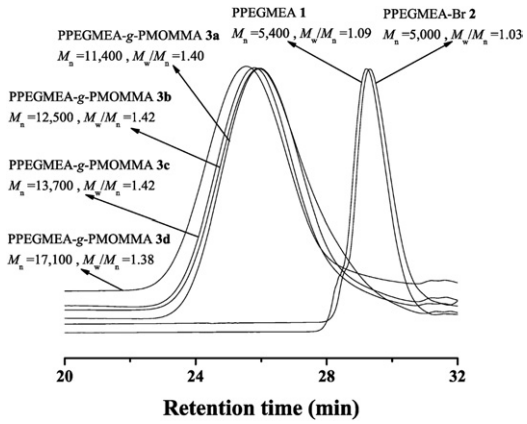

Fig. 1 GPC traces of PPEGMEA **1**, PPEGMEA-Br **2** and PPEGMEA-*g*-PMOMMA **3** in THF.

ATRP can be evidenced from the unimodal and symmetrical GPC curve (Fig. 1) with narrow molecular weight distribution ($M_w/M_n = 1.09$). The feed ratio of macromonomer to initiator was 20 : 1. The theoretical molecular weight of the comb homopolymer PPEGMEA **1** can be estimated from the conversion of macromonomer, which is 100% for the current case. The real molecular weight of PPEGMEA **1** was calculated to be 9100 from ^{1}H NMR. This is in accordance with the theoretical value. We could thus conclude that every PPEGMEA **1** polymer chain possesses *ca.* 20 poly(ethylene glycol) side chains.

In the present study, poly(ethylene glycol) side chains are connected to the polyacrylate backbone by the ester groups. Instead, ATRP initiation groups have to be connected to the α-carbon of the ester groups of the polyacrylate backbone using lithium diisopropylamine (LDA) and 2-bromopropionyl chloride as shown in Scheme 1. CHBr groups of ATRP initiation groups, ester groups and CHBr end groups of PPEGMEA **1** are not affected during the reaction, which has been evidenced from the previous reports.[40–42] By this newly developed method, all the ATRP initiation groups were connected to the polyacrylate backbone through stable C–C bonds instead of ester connections.

PPEGMEA-Br **2** was characterized by ^{1}H NMR and ^{13}C NMR. A new peak at 1.90 ppm, which belonged to 3 protons of the newly introduced –CH(CH_3)Br group, was found in ^{1}H NMR spectrum. But this peak was overlapped with the signals of the polyacrylate backbone. No signal from the alkene was found in the region between 4.5 ppm and 7.0 ppm, which meant that the possible elimination reaction of the CHBr end group did not occur during the reaction. Also, a new peak appeared at 211.1 ppm in the ^{13}C NMR spectrum, which was attributed to the ketone carbon of -*C*OCH(CH_3)Br. All this evidence confirmed the successful introduction of ATRP initiation groups.

Apart from NMR spectra, this product was further analyzed by elemental analysis. The approximate grafted ATRP initiation group density, in %, is calculated from element analysis results for carbon (C%) or bromine (Br%) according to the following equations:

$$C\% = 48.4\% \times In\% + 54.9\% \times (1 - In\%) \quad (1)$$

$$Br\% = 80 \times In\%/[590 \times In\% + 454 \times (1 - In\%)] \quad (2)$$

In eqn 1, 48.4% is the carbon content of the repeat units with ATRP initiation groups, 54.9% is the carbon content of the repeat units without ATRP initiation groups. The initiation group density, In%, is calculated to be 74.5% according to eqn 1. In eqn 2, 590 is the molecular weight of the repeat units with ATRP initiation groups and 454 is the molecular weight of the repeat units without ATRP initiation groups. According to eqn 2, In% is calculated to be 68.9%. These two results were quite close to each other, but the first one calculated from the carbon content is more reliable due to the definition of the analysis method. Therefore, about 20 × 74.5% = 15 ATRP initiation groups were introduced onto the polyacrylate backbone.

As we can see from Fig. 1, only a unimodal and symmetric peak was observed from the GPC curve of PPEGMEA-Br **2** and the molecular weight distribution remained narrow (M_w/M_n = 1.03), this meant that the architecture of the polymer backbone was not altered during the reaction with LDA and 2-bromopropionyl chloride.[40–42] The M_n of PPEGMEA-Br **2** macroinitiator (M_n = 5000) was slightly smaller than that of PPEGMEA **1** (M_n = 5400), which is similar to our previous studies,[40–42] we could attribute this to the newly branched ATRP initiation groups.

Graft copolymerization of methoxymethyl methacrylate

ATRP of methoxymethyl methacrylate was performed in bulk to overcome the limitation of the slow reaction speed which is caused by the high initiation group density (74.5%) of PPEGMEA-Br **2** macroinitiator, this will however increase the possibility of inter-initiator coupling. Different ligands (PMDETA, HMTETA and Me_6TREN) as well as different polymerization temperatures (30 °C and 60 °C) were tested in order to optimize the polymerization conditions. The polymerization using PMDETA as a ligand at 60 °C was too slow and the polymerization using HMTETA as ligand was not successful. The most suitable polymerization conditions were to use Me_6TREN as a ligand at 30 °C. The results with different polymerization times under these condition are listed in Table 1.

It is clear that all the molecular weights of the obtained graft copolymers were much higher than that of the macroinitiator, this indicates the occurrence of the polymerization of MOMMA. The molecular weights of the graft copolymers increased linearly with the conversion of MMOMA, which is the characteristic of ATRP. GPC curves of PPEGMEA-*g*-PMOMMA **3** graft copolymers are also shown in Fig. 1. All the copolymers showed unimodal and symmetrical GPC curves with narrow molecular weight distributions ($M_w/M_n \leq 1.42$), which are characteristic of living polymerization and also indicated that intermolecular coupling reactions could be neglected under the current reaction conditions.[43] In the present study, a high feed ratio of monomer to initiator and a low conversion of monomer were used to suppress the intermolecular coupling reactions, this was the same as previous reports of the synthesis of linear graft copolymers.[43–47]

The structure of PPEGMEA-*g*-PMOMA **3** densely grafted copolymers was characterized by FT-IR and ^{1}H NMR. Fig. 2A shows the FT-IR spectrum of PPEGMEA-*g*-PMOMMA **3**. The typical signal of the –OCH_2O– group of the PMOMMA segment was found to appear at 918 cm^{-1}. The peaks at 1737, 1152 and 1075 cm^{-1} can be attributed to polyacrylate and PEG segments.

Table 1 Synthesis of PPEGMEA-*g*-PMOMMA graft copolymer[a]

	Time/h	M_n[b]/g mol^{-1}	M_w/M_n[b]	$M_{n,MALS}$[c]/g mol^{-1}	N_{MOMMA}[d]	Conv.[e] (%)	cmc[f]/g mL^{-1}
3a	6	11 400	1.40	27,600	9.49	7.90	1.08×10^{-6}
3b	8	12 500	1.42	29,300	10.36	10.67	8.11×10^{-7}
3c	10	13 700	1.42	33,900	12.72	12.16	1.06×10^{-6}
3d	12	17 100	1.38	35,200	13.38	15.99	1.33×10^{-6}

[a] Initiated by PPEGMEA **2** ($M_n = 5000$, $M_w/M_n = 1.03$, grafted ATRP initiation group density: 0.75/1), [MOMMA] : [Br group] : [CuBr] : [Me_6TREN] = 400 : 1 : 1 : 1.[b] Measured by GPC in THF.[c] Obtained by GPC/MALS in THF.[d] The number of MOMMA repeating units per PMOMMA side chain determined by GPC/MALS.[e] Conversion of MOMMA measured by GC.[f] Critical micelle concentration determined by fluorescence spectroscopy using PNA as a probe.

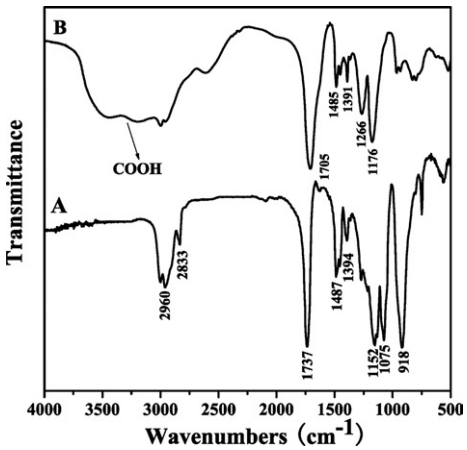

Fig. 2 FT-IR spectra of PPEGMEA-*g*-PMOMMA **3** (A) and PPEGMEA-g-PMAA **4** (B).

The ^{1}H NMR spectrum of PPEGMEA-*g*-PMOMA **3** is shown in Fig. 3A. The typical signals of PMOMMAs segment were found to appear at 3.41 and 5.17 ppm. The peaks at 3.50 and 3.60 ppm correspond to PEG side chains.

Generally, ^{1}H NMR spectra are used to determine the composition of the copolymer. But some previous studies showed that the ^{1}H NMR spectra of amphiphilic copolymers were affected by the conditions of the measurement.[43,48–50] In our recent work, it was found that the compositions of amphiphilic densely grafted copolymers obtained from ^{1}H NMR spectra were dependent on the conditions of the measurements due to their complex structure.[30] Since it was difficult to determine the "actual" composition of PPEGMEA-*g*-PMMOMA **3** by ^{1}H NMR, the absolute molecular weight of PPEGMEA-*g*-PMMOMA **3** was measured by GPC/MALS in THF instead.

From the molecular weight of PPEGMEA **1** ($M_n = 9100$) and the absolute molecular weight of PPEGMEA-*g*-PMMOMA **3** determined by GPC/MALS, the number of MMOMA repeating units per PMMOMA side chain (N_{MOMMA}) was calculated according to eqn 3 as listed in Table 1:

$$N_{MMOMA} = (M_{n,MALS} - 9100)/(15 \times 130) \quad (3)$$

The semilogarithmic plot of $\ln([M]_0/[M])$ *vs.* time, as depicted in Fig. 4, shows that the conversion of MOMMA increases with the time and a linear dependence of $\ln([M]_0/[M])$ on the time. It shows first order polymerization kinetics demonstrating a constant number of propagating species during the polymerization, which is a typical characteristic of ATRP.

From the above results, it can be concluded that the polymerization of the backbone and side chains were both controllable. The obtained copolymer, PPEGMEA-*g*-PMOMMA **3**, is a little different to our previously reported centipede-like copolymer since the graft density of PMOMMA is only 75%, here we call it a densely grafted copolymer with well-defined structure (Scheme 1): a polyacrylate backbone (20 repeating units) with two side chains, one is short PEG (8.4 repeating units

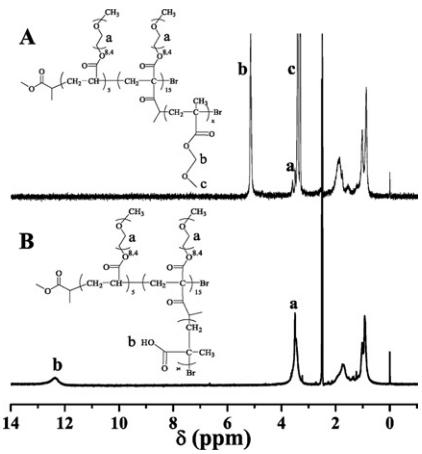

Fig. 3 ^{1}H NMR spectra of PPEGMEA-*g*-PMOMMA **3** (A) and PPEGMEA-*g*-PMAA **4** (B) in DMSO-d_6.

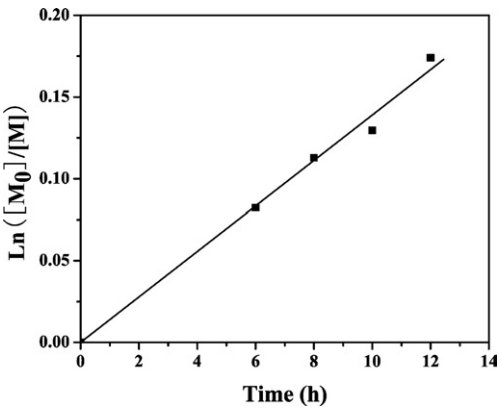

Fig. 4 Kinetic plot for bulk ATRP of MOMMA initiated by PPEGMEA-Br **2**.

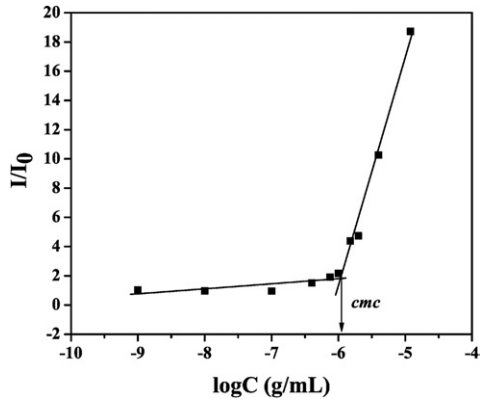

Fig. 5 Dependence of the fluorescence intensity ratio of the PNA emission band at 418 nm on the concentration of PPEGMEA-*g*-PMMOMA **3a**.

per chain) at each grafting point, the other is PMOMMA (9.49–13.38 repeating units per chain) at most grafting points.

Critical micelle concentration of PPEGMEA-*g*-PMOMMA 3

The critical micelle concentrations of PPEGMEA-*g*-PMOMMA **3** amphiphilic graft copolymer in aqueous solution were determined by fluorescence techniques using PNA as a fluorescence probe (Fig. 5). PNA was a more suitable fluorescent probe than pyrene in terms of reproducibility since it displays higher fluorescence activity in nonpolar environments and it can be very easily quenched by polar solvents such as water.[51] The measured cmc values of the micelles of PPEGMEA-*g*-PMOMMA **3** are listed in Table 1. We could see that the length of the PMOMMA side chains can only slightly affect the cmc values.

From the data in Table 1, the cmc of the graft copolymer does not show a clear relationship with the length of the PMOMMA side chains. These cmc values are higher than those of the amphiphilic centipede-like copolymer PPEGMEA-*g*-PS we reported before,[30] which means that PMOMMA side chains are less hydrophobic than polystyrene side chains. The lower hydrophobicity may be attributed to the hydrogen bonds between the ether groups and water.

Properties of micelles formed by PPEGMEA-*g*-PMOMMA 3

The micelle structure was explored by TEM. The typical TEM images of micelles formed by the PPEGMEA-*g*-PMOMA **3** amphiphilic graft copolymer are shown in Fig. 6. The micelles formed by PPEGMEA-*g*-PMOMMA **3** with different molecular weights are large compound micelles.

Hydrolysis of PMOMMA side chains

The methoxymethyl groups of PPEGMEA-*g*-PMOMMA can be easily hydrolyzed by 1M HCl without affecting the polyacrylate backbone, this process is highly efficient and selective. The resulting product, PPEGMEA-*g*-PMAA **4**, is water-soluble. Results from FT-IR analysis confirmed the presence of methacrylic acid groups, as one can see from Fig. 2B, after hydrolysis, a broad absorbance appeared at 2800–3600 cm^{-1} which is characteristic of a carboxylic acid group; meanwhile, the

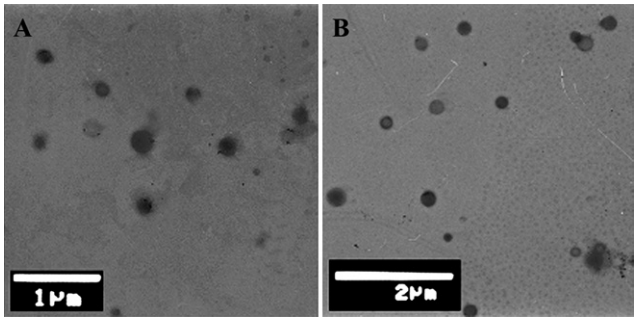

Fig. 6 TEM images of micelles formed by PPEGMEA-*g*-PMOMMA **3a** (A) and **3d** (B).

peak of the $–OCH_2O–$ group at 918 cm^{-1} disappeared and the peak of the carbonyl shifted from 1737 cm^{-1} to 1705 cm^{-1}. Fig. 3B shows ^1H NMR spectrum of the graft copolymer after hydrolysis. The complete disappearance of the characteristic strong peaks of the $–OCH_2OCH_3$ group at 3.41 ppm and 5.17 ppm demonstrates the successful hydrolysis of the PMOMMA side chains. The new signal at 12.33 ppm further confirmed the formation of the PMAA segment.

The solubility of PPEGMEA-*g*-PMAA **4** was checked in pH-adjusted water. It was found that PPEGMEA-*g*-PMAA **4** precipitated in water when pH<4.0. However, PPEGMEA-*g*-PMAA **4** shows poor solubility in the range 4.0<pH<6.0 and good solubility when pH>6.0 since PMAA is a weak acid and soluble under basic conditions.

Preparation and characterization of Fe_3O_4/polymer nano-composite

The chemical co-precipitation of ferric and ferrous salts is a common method to prepare Fe_3O_4 nano-particles as shown in Scheme 2.[52]

Fe_3O_4 nano-particles synthesized by this approach are easy to aggregate due to the interaction of the particles.[52] PPEGMEA-*g*-PMAA **4** densely grafted double hydrophilic copolymers might be able to prevent the unfavorable aggregation since the side chains can serve to protect the formed single particles. To test this, PPEGMEA-*g*-PMAA **4** was used as a template to prepare Fe_3O_4/polymer nano-composites employing this conventional chemical co-precipitation method. The results are listed in Table 2.

With this graft copolymer as the template, the obtained Fe_3O_4/polymer nano-composites are stable in water and can suspend in water homogeneously. The proposed mechanism is shown in Scheme 3.

Fe^{2+} and Fe^{3+} cations were coordinated with carboxylic acid groups along the PMAA side chains to form the complexes at the beginning. The nucleation of Fe_3O_4 particles were prompted by carboxylic acid groups of PMAA side chains in the presence of NaOH aqueous solution.[37–39] In the current system, PMAA side chains bearing carboxylic acid groups acted as venues for the

$$Fe^{2+} + 2Fe^{3+} + 8OH^- \xrightarrow{N_2} Fe(OH)_2 + 2Fe(OH)_3 \xrightarrow[\triangle]{N_2} Fe_3O_4 + H_2O$$

Scheme 2 Synthesis of Fe_3O_4 nano-particles by chemical co-precipitation.

Table 2 Characterization of the Fe_3O_4/polymer nano-composite

Sample	Polymer	R_p[a]	D_h[b]/nm	PI[b]	Weight loss[c] (%)	ζ potential[b]/mV	$L_{Fe_3O_4}$[d] /nm
NP-1	—	—	210	0.13	6.8	−0.377	13.4
CNP-2	**4d**	1/1	189	0.194	23.2	−43.6	10.4
CNP-3	**4d**	1/2	173	0.20	20.3	−41.5	9.5
CNP-4	**4d**	1/3	184	0.149	18.9	−37.7	8.5
CNP-5	**4a**	1/2	52.7	0.290	10.3	−35.7	8.1
CNP-6	**4c**	1/2	57.1	0.243	14.4	−40.8	8.3

[a] The weight ratio of copolymer to Fe_3O_4 nano-particle used.[b] Measured by DLS.[c] Determined by TGA.[d] Crystal size of Fe_3O_4 calculated from XRD data.

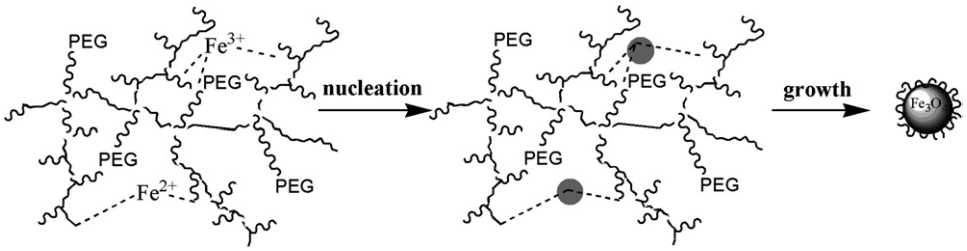

Scheme 3 Synthesis of Fe_3O_4/polymer nano-composite in the presence of PPEGMEA-*g*-PMAA **4** densely grafted double hydrophilic copolymer

nucleation of Fe_3O_4 nano-particles, while PEG side chains retarded the growth of Fe_3O_4 nano-particles by the so-called shielding effect, which resulted in nano-particles with smaller sizes (8.0–10.5 nm). The sizes were calculated from XRD data using the Scherrer equation and are listed in Table 2.

The Fe_3O_4/polymer nano-composites were characterized by FT-IR. Fig. 7 shows the FT-IR spectra of the PPEGMEA-*g*-PMAA **4** graft copolymer, native Fe_3O_4 nano-particles and Fe_3O_4/polymer nano-composites. It was reported that the characteristic absorption band of the Fe–O bond in bulk Fe_3O_4 appears at 570 cm^{-1}.[53] However, when the size of the Fe_3O_4 particle decreased to nano-scale dimensions, the surface bond force constant would increase dramatically due to the finite size effect of nano-particles, in which the breaking of a large number of bonds for atoms on the surface will result in the rearrangement of non-localized electrons on the surface.[54] The FT-IR spectrum of native Fe_3O_4 nano-particles thus exhibits a blue shift for the characteristic absorption band of Fe–O bond positioned at 575 cm^{-1} as shown in Fig. 7B.

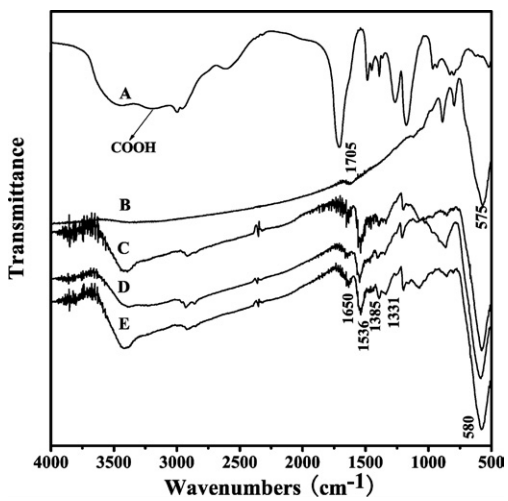

Fig. 7 FT-IR spectra of PPEGMEA-*g*-PMAA **4** (A), native Fe_3O_4 nano-particle NP-1 (B), Fe_3O_4/polymer nano-composites CNP-2 (C), CNP-3 (D) and CNP-4 (E).

Fig. 7C, 7D and 7E show the FT-IR spectra of Fe_3O_4/polymer nano-composites coated with different amounts of graft copolymer. The characteristic absorption bands of the Fe–O bond are found to appear at 580 cm^{-1} in all 3 spectra. The broad band of the carboxyl group of the PMAA side chains between 3000 cm^{-1} to 3600 cm^{-1} diminished and the peaks of the carbonyls at 1650 cm^{-1} and 1536 cm^{-1} faded too. The peak at 1650 cm^{-1} indicated that a part of the PMAA segments were ligated to Fe_3O_4 nano-particles in mono-dentate form.[55] At the same time, two new peaks appeared at 1385 cm^{-1} and 1331 cm^{-1} due to the binding of carboxyls to the surface of Fe_3O_4 nano-particles to form carboxylate groups, these new peaks arose from asymmetric and symmetric vibrations of carboxylate groups and demonstrated the bi-dentate bonding to Fe atoms on the surface.[56,57]

The crystal structure of Fe_3O_4/polymer nano-composite was investigated by XRD. Only six characteristic peaks ($2\theta = 29.8°$, 35.1°, 42.9°, 53.1°, 56.7°, 62.4°) of standard Fe_3O_4 crystals (isometric-hexoctahedral crystal system)[58] are found in the diffraction pattern as shown in Fig. 8, which illustrated the absence of other magnetic, crystalline iron oxide species.

The sizes of microcrystals can be quantitatively evaluated from XRD data using the Scherrer equation as listed in Table 2, which gives a relationship between peak width and particle size.[59] The sizes descended with the decreasing quantity of graft copolymer; on the other hand, the particles prepared from the graft copolymer with shorter PMAA side chains have a smaller size. Thus, it can be concluded that the particle size can be tuned by the weight

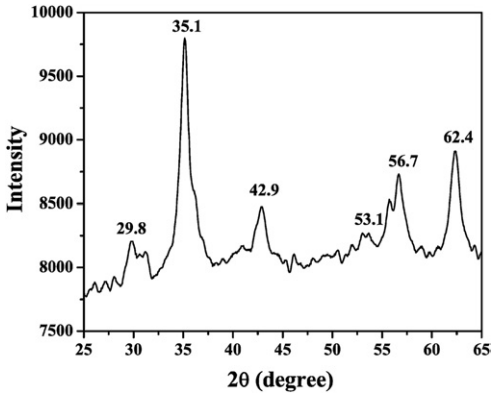

Fig. 8 XRD pattern of the Fe_3O_4/polymer nano-composite CNP-2.

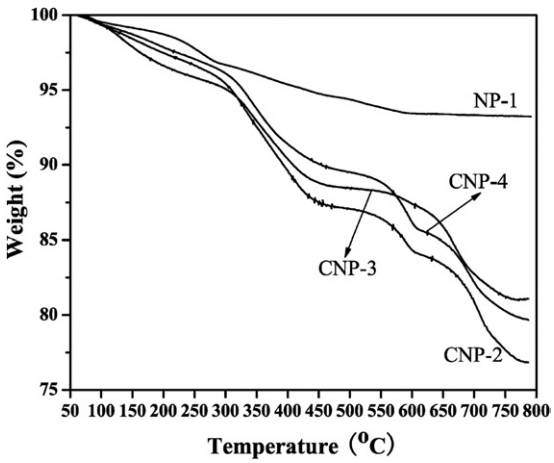

Fig. 9 TGA curves of pure Fe_3O_4 nano-particles and Fe_3O_4/polymer nano-composites.

ratio of copolymer to Fe_3O_4 nano-particle used and the length of the PMAA side chains.

The thermal properties of Fe_3O_4/polymer nano-composites were studied by TGA. As shown in Fig. 9, native Fe_3O_4 nano-particles have only a tiny weight loss between 50 °C and 800 °C, while three stages were found in the TGA curves of Fe_3O_4/polymer nano-composites by contrast. The weight loss first took place at below 300 °C, which can be attributed to either the evaporation of trace water or the decomposition of non-coordinated carboxyls. The weight loss between 300 °C and 450c °C arose from the cleaving of the PEG side chains. The decomposition of coordination between PMAA segments and Fe_3O_4 nano-particle started above 450 °C in the final stage. The residual weight of nano-composite is clearly contributed from the Fe_3O_4 nano-particle. Based on the above analysis, the decompositions of PEG and PMAA side chains of graft copolymers are the main origins for the weight loss of Fe_3O_4/polymer nano-composites. The TGA results listed in Table 2 show that the weight percentage of coated graft copolymer in nano-composite rose when the weight ratio of used graft copolymer to Fe_3O_4 nano-particle increased. Moreover, the weight percentage of coated graft copolymer in the nano-composite increased with the increase in the length of the PMAA side chains due to the enhancement of the coordination between the carboxyls and Fe_3O_4 nano-particles.

ξ potentials can demonstrate the magnitude of the repulsion or attraction between the particles and can also provide a detailed insight into the dispersion mechanism. ξ potential measurements listed in Table 2 revealed that all nano-composites have a net negative charge which is proportional to the weight ratio of graft copolymer to Fe_3O_4 nano-particle used. On the other hand, the charge is also relevant to the length of the PMAA side chains. This result further confirmed the presence of negatively charged graft copolymers on the surface of the Fe_3O_4 nano-particle.[38]

DLS studies demonstrated that all Fe_3O_4/polymer nano-composites have smaller hydrodynamic diameters (D_h) than that of native Fe_3O_4 nano-particles. This implies that Fe_3O_4 nano-particles can be dispersed by PPEGMEA-*g*-PMAA **4** double hydrophilic graft copolymers. The narrow size distributions of the nano-composites indicated that the sizes are almost identical. It is clear that the sizes of nano-composites are also influenced by the weight ratio of used graft copolymer to Fe_3O_4 nano-particle. When the weight ratio of copolymer **4d** to Fe_3O_4 nano-particle varied from 1/1 to 1/3, the D_h of nano-composite decreased from 189 nm to 173 nm followed by an increase from 173 nm to 184 nm. It is clear that a suitable weight ratio of used graft copolymer to Fe_3O_4 nano-particle is 1/2, which leads to the best dispersion. Under this condition, Fe_3O_4/polymer nano-composites coated with graft polymers with shorter PMAA side chains will possess smaller hydrodynamic diameters, this means that graft polymers with shorter PMAA side chains can also prevent the aggregation and disperse Fe_3O_4 nano-particle very well.

Fe_3O_4/polymer nano-composites were also examined by TEM as shown in Fig. 10. Only Fe_3O_4 nano-particles can be observed while the associated graft copolymers cannot be observed. The diameters of Fe_3O_4 nano-particles were about 7–15 nm, which were similar to the results calculated from XRD data.

Fig. 10A, 10B and 10C show the aggregated clusters when the graft copolymer with longer PMAA side chains was used as a template to prepare nano-composites. Although these monocrystalline spheres were closely packed together, they were still distinctively separated with clear boundaries. Interestingly, Fe_3O_4 nano-particles can still be well dispersed as shown in Fig. 10D and 10E when the graft copolymers with shorter PMAA side chains were used as the template. This is due to a weaker coordinating ability of shorter PMAA side chains and has been proved by the increasing ξ potentials as listed in Table 2.

In summary, the size and dispersion of Fe_3O_4/polymer nano-composite can be tuned by the weight ratio of graft polymer to Fe_3O_4 nano-particle used and the length of the PMAA side chains.

Magnetic properties of Fe_3O_4/polymer nano-composite

The magnetic properties of the Fe_3O_4/polymer nano-composites were explored by a vibrating sample magnetometer at room temperature. Fig. 11 shows the magnetization curves of pure Fe_3O_4 nano-particles and Fe_3O_4/polymer nano-composites. It was found that all Fe_3O_4/polymer nano-composites were superparamagnetic since neither remanence nor coercivity was measured at room temperature when the magnetic filed was removed, which is similar to previous literature.[36]

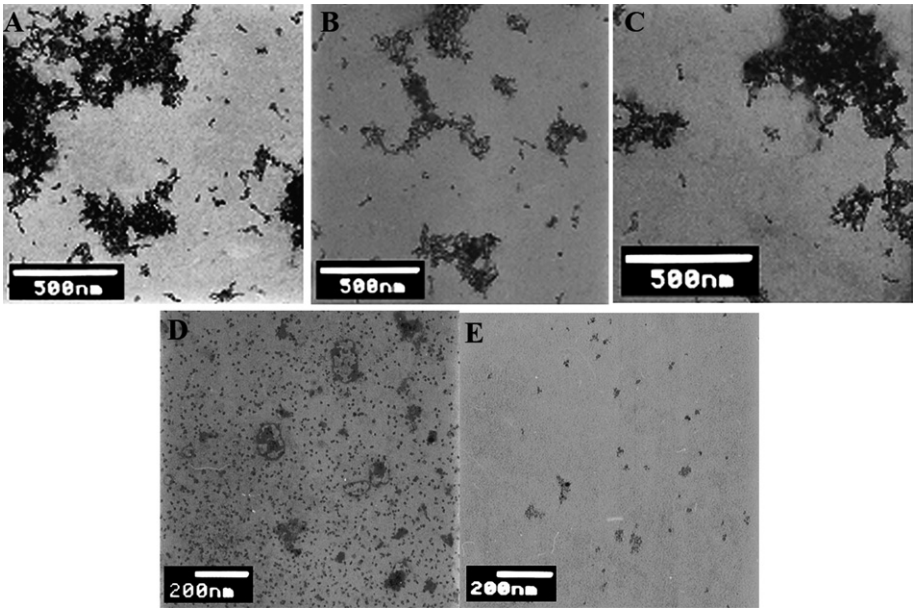

Fig. 10 TEM images of Fe_3O_4/polymer nano-composites CNP-2 (A), CNP-3 (B), CNP-4 (C), CNP-5 (D) and CNP-6 (E).

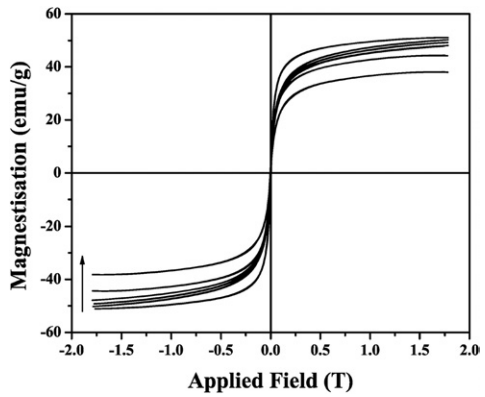

Fig. 11 Magnetization curves of native Fe_3O_4 nano-particles and Fe_3O_4/polymer nano-composites, from bottom to top: NP-1, CNP-2, CNP-3, CNP-4, CNP-6 and CNP-5.

Superparamagnetic particles no longer show magnetic interactions after the elimination of the magnetic field, and therefore the aggregation between the particles could be reduced. The saturation magnetization (M_s) and the coercivity (H_c) of pure Fe_3O_4 nano-particles and Fe_3O_4/polymer nano-composites are summarized in Table 3.

The saturation magnetizations (M_s) of all these nano-particles were above 38 emu g^{-1}, which are comparable to the reported values.[34–36] Since the particle sizes were close, no obvious loss of saturation magnetization was observed between Fe_3O_4/polymer nano-composites and bare Fe_3O_4 magnetite nano-particle. This result demonstrated that polymeric templates did not affect the magnetization properties of the Fe_3O_4 nano-particles. In addition, it was found that saturation magnetizations (M_s) decreased continuously with the descending particle sizes, which is similar to previous literature.[36] Thus, it can be predicted that the magnetic properties of Fe_3O_4/polymer nano-composites evolve gradually as a function of particle size.

Table 3 Magnetic properties of Fe_3O_4/polymer nano-composite

Sample	Polymer	R_p[a]	$L_{Fe_3O_4}$[b]/nm	M_s[c]/emu g^{-1}	H_c[c]/mT
NP-1	—	—	13.4	51.1	3.8
CNP-2	**4d**	1/1	10.4	50.3	1.3
CNP-3	**4d**	1/2	9.5	49.2	1.8
CNP-4	**4d**	1/3	8.5	48.0	1.6
CNP-5	**4a**	1/2	8.1	38.2	1.7
CNP-6	**4c**	1/2	8.3	44.4	1.7

[a] The weight ratio of used copolymer to Fe_3O_4.[b] Crystal Size of Fe_3O_4 calculated from XRD data.[c] Determined by VSM at room temperature.

From the above results, it is clear that Fe_3O_4/polymer nano-composites show superparamagnetic behavior at room temperature and the magnetic properties of Fe_3O_4/polymer nano-composites evolve gradually as a function of particle size.

Conclusion

A series of well-defined amphiphilic densely grafted copolymers containing two different side chains were synthesized by a combination of ATRP and the grafting-from strategy. The molecular weights of both the backbone and the side chains were controllable and the molecular weight distributions were in the range 1.38–1.42. Hydrophobic PMOMMA side chains were connected to the backbone through stable C–C bonds instead of ester connections and they can be selectively hydrolyzed under mild conditions with high efficiency to obtain a new class of double hydrophilic densely grafted copolymer consisting of two different hydrophilic side chains of PEG and PMAA.

Fe_3O_4/polymer nano-composites with narrow size distributions were prepared *via* an *in situ* co-precipitation process using these double hydrophilic densely grafted copolymers as a template, which provided a good choice for preparing stable nano-composites with PEG-modified surfaces. The size and

dispersion of the nano-composites can be tuned by the length of the PMAA side chains and the weight ratio of graft copolymer to Fe_3O_4 nano-particle used. The nano-composites showed superparamagnetic behavior at room temperature, which implies potential applications in the biomedical field.

Acknowledgements

The authors thank the financial support from National Natural Science Foundation of China (20404017), Shanghai Nano-Technology Program (0652nm031), Shanghai Rising Star Program (07QA14066) and the Knowledge Innovation Program of the Chinese Academy of Sciences.

References

1 H. Colfen, *Macromol. Rapid Commun.*, 2001, **22**, 219.
2 T. J. Martin, K. Prochazka, P. Munk and S. E. Webber, *Macromolecules*, 1996, **29**, 6071.
3 A. S. Lee, A. P. Gast, V. Butun and S. P. Armes, *Macromolecules*, 1999, **32**, 4302.
4 J. F. Gohy, S. Creutz, M. Garsia, B. Mahltig, M. Stamm and R. Jerome, *Macromolecules*, 2000, **33**, 6378.
5 E. Khousakoun, J. F. Gohy and R. Jerome, *Polymer*, 2004, **45**, 8303.
6 J. F. Gohy, S. K. Varshney and R. Jerome, *Macromolecules*, 2001, **34**, 3361.
7 X. H. Guo, S. H. Yu and G. B. Cai, *Angew. Chem., Int. Ed.*, 2006, **45**, 3977.
8 M. Vamvakaki, D. Palioura, A. Spyros, S. P. Armes and S. H. Anastasiadis, *Macromolecules*, 2006, **39**, 5106.
9 X. Andre, M. F. Zhang and A. H. E. Muller, *Macromol. Rapid Commun.*, 2005, **26**, 558.
10 G. Mountrichas and S. Pispas, *Macromolecules*, 2006, **39**, 4767.
11 X. S. Wang, R. A. Jackson and S. P. Armes, *Macromolecules*, 2000, **33**, 255.
12 Z. S. Ge, Y. L. Cai, J. Yin, Z. Y. Zhu, J. Y. Rao and S. Y. Liu, *Langmuir*, 2007, **23**, 1114.
13 K. Tsutsumiuchi, K. Aoi and M. Okada, *Macromol. Rapid Commun.*, 1995, **16**, 749.
14 C. Forder, C. S. Patrickios, S. P. Armes and N. C. Billingham, *Macromolecules*, 1997, **30**, 5758.
15 Y. Cai, Y. Tang and S. P. Armes, *Macromolecules*, 2004, **37**, 9728.
16 S. Forster and T. Plantenberg, *Angew. Chem., Int. Ed.*, 2002, **41**, 688.
17 J. S. Wang and K. Matyjaszewski, *J. Am. Chem. Soc.*, 1995, **117**, 5614.
18 J. S. Wang and K. Matyjaszewski, *Macromolecules*, 1995, **28**, 7901.
19 V. Percec and B. Barboiu, *Macromolecules*, 1995, **28**, 7970.
20 M. Kato, M. Kamigaito, M. Sawamoto and T. Higashimura, *Macromolecules*, 1995, **28**, 1721.
21 W. Jakubowski and K. Matyjaszewski, *Angew. Chem., Int. Ed.*, 2006, **45**, 4482.
22 J. K. Oh, K. Min and K. Matyjaszewski, *Macromolecules*, 2006, **39**, 3161.
23 V. Percec, T. Guliashvili, J. S. Ladislaw, A. Wistrand, A. Stjerndahl, M. J. Sienkowska, M. J. Monteiro and S. Sahoo, *J. Am. Chem. Soc.*, 2006, **128**, 14156.
24 J. F. J. Coelho, A. M. F. P. Silva, A. V. Popov, V. Percec, M. V. Abreu, P. M. O. F. Goncalves and M. H. Gil, *J. Polym. Sci., Part A: Polym. Chem.*, 2006, **44**, 3001.
25 D. Neugebauer, Y. Zhang, T. Pakula, S. Sheiko and K. Matyjaszewski, *Macromolecules*, 2003, **36**, 6746.
26 D. Neugebauer, Y. Zhang, T. Pakula and K. Matyjaszewski, *Polymer*, 2003, **44**, 6863.
27 H. Iatrou, J. W. Mays and N. Hadjichristidis, *Macromolecules*, 1998, **31**, 6697.
28 S. W. Ryu, H. Asada and A. Hirao, *Macromolecules*, 2004, **37**, 6291.
29 A. X. Li, Z. J. Lu, Q. F. Zhou, F. Qiu and Y. L. Yang, *J. Polym. Sci., Part A: Polym. Chem.*, 2006, **44**, 3942.
30 L. N. Gu, Z. Shen, S. Zhang, G. L. Lu, X. H. Zhang and X. Y. Huang, *Macromolecules*, 2007, **40**, 4486.
31 M. J. Roberts, M. D. Bentley and J. M. Harris, *Adv. Drug Delivery Rev.*, 2002, **54**, 459.
32 F. M. Veronese, *Biomaterials*, 2001, **22**, 405.
33 J. Pyun, *Polym. Rev.*, 2007, **47**, 231.
34 H. Lee, E. Lee, D. K. Kim, N. K. Jang, Y. Y. Jeong and S. Y. Jon, *J. Am. Chem. Soc.*, 2006, **128**, 7383.
35 R. Abu-Much, U. Meridor, A. Frydman and A. Gedanken, *J. Phys. Chem. B*, 2006, **110**, 8194.
36 S. R. Wan, J. S. Huang, H. S. Yan and K. L. Liu, *J. Mater. Chem.*, 2006, **16**, 298.
37 M. F. Zhang, C. Estourne, W. Bietsch and A. H. E. Muller, *Adv. Funct. Mater.*, 2004, **14**, 871.
38 J. F. Lutz, S. Stiller, A. Hoth, L. Kaufner, U. Pison and R. Cartier, *Biomacromolecules*, 2006, **7**, 3132.
39 G. D. Moeser, W. H. Green, P. E. Laibinis, P. Linse and T. A. Hatton, *Langmuir*, 2004, **20**, 5223.
40 D. Peng, X. H. Zhang and X. Y. Huang, *Macromolecules*, 2006, **39**, 4945.
41 D. Peng, C. Feng, G. L. Lu, S. Zhang, X. H. Zhang and X. Y. Huang, *J. Polym. Sci., Part A: Polym. Chem.*, 2007, **45**, 3687.
42 D. Peng, G. L. Lu, S. Zhang, X. H. Zhang and X. Y. Huang, *J. Polym. Sci., Part A: Polym. Chem.*, 2007, **45**, 6857.
43 G. Cheng, A. Boker, M. Zhang, G. Krausch and A. H. E. Muller, *Macromolecules*, 2001, **34**, 6883.
44 K. Matyjaszewski, S. Qin, J. R. Boyce, D. Shirvanyants and S. S. Sheiko, *Macromolecules*, 2003, **36**, 1843.
45 S. Liu and S. Ayusman, *Macromolecules*, 2000, **33**, 5106.
46 Z. Shen, Y. Chen, E. Barriau and H. Frey, *Macromol. Chem. Phys.*, 2006, **207**, 57.
47 M. Zhang, T. Breiner, H. Mori and A. H. E. Muller, *Polymer*, 2003, **44**, 1449.
48 S. Angot, D. Taton and Y. Gnanou, *Macromolecules*, 2000, **33**, 5418.
49 S. Liu, J. V. M. Weaver, Y. Tang, N. C. Billingham, S. P. Armes and K. Tribe, *Macromolecules*, 2002, **35**, 6121.
50 D. Li, X. Sheng and B. Zhao, *J. Am. Chem. Soc.*, 2005, **127**, 6248.
51 L. C. You, F. Z. Lu, Z. C. Li, W. Zhang and F M. Li, *Macromolecules*, 2003, **36**, 1.
52 R. Kaiser and G. Miskolczy, *J. Appl. Phys.*, 1970, **41**, 1064.
53 R. D. Waldron, *Phys. Rev.*, 1955, **99**, 1727.
54 M. Ma, Y. Zhang, W. Yu, H. Y. Shen, H. Q. Zhang and N. Gu, *Colloids Surf., A: Physicochem. Eng. Asp.*, 2003, **212**, 219.
55 N. Kohler, G. E. Fryxell and M. Q. Zhang, *J. Am. Chem. Soc.*, 2004, **126**, 7206.
56 R. G. C. Moore, S. D. Evans, T. Shen and C. E. C. Hodson, *Physica E*, 2001, **9**, 253.
57 Q. X. Liu and Z. H. Xu, *Langmuir*, 1995, **11**, 4617.
58 C. L. Lin, C. F. Lee and W. Y. Chiu, *J. Colloid Interface Sci.*, 2005, **291**, 411.
59 B. D. Cullity, *Elements of X-ray Diffraction*, Addison-Wesley, Reading, MA, 2nd edn, 1978, p. 102.

